

Radiative association of atomic hydrogen with antihydrogen at subkelvin temperatures

B. Zygelman

Department of Physics, University of Nevada, Las Vegas, Las Vegas, Nevada 89154

Alejandro Saenz

Max Planck Institute for Quantum Optics, Hans Kopfermann Straße 1, D-85748 Garching, Germany

P. Froelich and S. Jonsell

Department of Quantum Chemistry, Uppsala University, Box 518, 75120 Uppsala, Sweden

A. Dalgarno

Harvard-Smithsonian Center for Astrophysics, 60 Garden Street, Cambridge, Massachusetts 02138

(Received 23 May 2000; published 19 April 2001)

Partial and total cross sections for the radiative association process $H + \bar{H} \rightarrow H\bar{H} + h\nu$ in the sub-Kelvin temperature regime are reported. We calculate the emission spectra for this process and suggest its utility as a diagnostic. The cross section for radiative association is found to have the value $\sigma = 6.85 \times 10^{-22} \text{ cm}^2/\sqrt{T}$, where T is an effective temperature. It is significantly smaller than the in-flight annihilation and fragmentation cross sections. We discuss the role that radiative association plays in the formation of a quasibound system of the $H\bar{H}$ molecule.

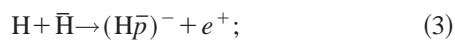
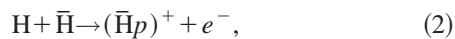
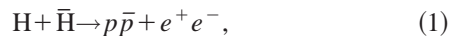
DOI: 10.1103/PhysRevA.63.052722

PACS number(s): 34.10.+x, 34.90.+q, 36.10.-k

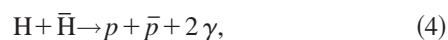
I. INTRODUCTION

The bound state of a positron and antiproton, the antihydrogen atom, has the special significance of occupying the first row and period of the antiperiodic table. Its detection has, until recently [1], remained elusive, but with the CERN antiproton decelerator (AD) coming on line it is anticipated that antihydrogen atoms will be created, cooled and stored in large numbers [2]. High-precision spectroscopic studies of the trapped antihydrogen promise to provide new tests and bounds for CPT violation and the weak equivalence principle (WEP) [2].

The cooling of the trapped antihydrogen gas is crucial for enabling high-precision spectroscopy of the \bar{H} atom. One proposed [3,4] cooling scheme involves the introduction of a cold buffer gas, such as ultracold, spin-polarized hydrogen into the sample of the \bar{H} gas. Elastic collisions among the hydrogen and antihydrogen atoms can thermalize and cool the antihydrogen, but inelastic collisions may limit the utility of this scheme at ultracold temperatures. Several inelastic collision channels can be accessed and they can be partitioned into the families of (i) rearrangement channels



(ii) in-flight annihilation channels whose decay products can be gamma-ray photons γ , or subnuclear fragments in the case of $p\bar{p}$ annihilation,



and (iii) spontaneous radiative decay channels



where $H\bar{H}$ is a quasibound molecular system consisting of the baryon and lepton matter and antimatter pair. This list is not exhaustive, but it is believed that process (1) is the dominant loss channel. Estimates of its cross section, and of the elastic channel cross sections, have been reported [4–11]. The most recent calculation [4,5] suggests that process (1) limits the utility of the sympathetic cooling of \bar{H} by cold H atoms to temperatures above a fraction of a Kelvin. In this paper, we present the results of a study of the radiative decay process (6). We find that it is allowed in the dipole approximation, in contrast to collisions of two hydrogen atoms since, in the latter, single-photon electric-dipole spontaneous decay is forbidden. The results of our calculation provide an effective cross section given by the formula $\sigma = 6.85 \times 10^{-22} \text{ cm}^2/\sqrt{T}$, where T is an effective temperature expressed in units of kelvin. We define the effective temperature by the relation $E \equiv \kappa T$, where E is the center-of-mass frame collision energy and κ the Boltzmann constant.

The cross section is smaller than that for the dominant rearrangement reaction (1) or the in-flight annihilation cross section, and we conclude that process (6) does not play a role in the kinetics of a dilute gas at ultralow temperatures.

Despite the fact that our studies suggest that process (6) plays a minor role in gas kinetics, the emitted radiation could serve as a valuable diagnostic of hydrogen atom–antihydrogen interactions. We present the emission spectrum

for this process and show that it ranges from hard x-ray radiation to the microwave band. Present capabilities for antihydrogen detection involve gamma rays in coincidence with particle fragment detectors [2]. Here we point out that process (6) provides a detection signal for antihydrogen in that part of the spectrum that lends itself to sensitive atomic and molecular photon detection methods. The spectrum could have applications in both laboratory studies and astronomical observations.

In Sec. II, we present the theory used in our calculations, and in Sec. III we provide both a qualitative description and quantitative calculation for the dipole moment induced by the slow approach of H with $\bar{\text{H}}$. In Sec. IV, we report the results of our calculation for the cross sections as well as the photon-emission spectra. We present additional discussion and a conclusion. Atomic units, unless otherwise stated, are used throughout.

II. THEORY

The cross section for the radiative process $\text{H} + \bar{\text{H}} \rightarrow \text{H}\bar{\text{H}} + h\nu$ is calculated using an expression derived within the dipole approximation [12],

$$\sigma(k) = \sum_J \sum_n \frac{64}{3} \frac{\pi^5 \nu^3}{c^3 k^2} [(J+1)M_{J+1,J}^2 + JM_{J-1,J}^2], \quad (7)$$

where the sum extends over the rovibrational quantum numbers n and J of the bound levels of the $\text{H}\bar{\text{H}}$ complex. The frequency ν of the emitted photon is $2\pi\nu = k^2/2\mu - E_{nJ}$, where k is the wave number corresponding to the relative motion of H and $\bar{\text{H}}$ during their initial approach, μ is the nuclear reduced mass of the $\text{H}\bar{\text{H}}$ system, and E_{nJ} is the energy eigenvalue for rovibrational level (n, J) of the $\text{H}\bar{\text{H}}$ complex. The transition dipole matrix element $M_{J,J'}$ is defined by

$$M_{J,J'} = \int_0^\infty dR f_J(kR) D(R) \phi_{J'}^n(R), \quad (8)$$

where $f_J(kR)$ is a radial continuum function of the $\text{H}-\bar{\text{H}}$ separation R that is a solution to the Schrödinger equation

$$\left\{ \frac{d^2}{dR^2} - \frac{J(J+1)}{R^2} - 2\mu[V(R) - V(\infty)] + k^2 \right\} f_J(kR) = 0. \quad (9)$$

In Eqs. (8) and (9), $V(R)$ is the potential-energy curve for the ground leptonic state of the $\text{H}\bar{\text{H}}$ molecular state, $D(R)$ is the radial electric-dipole moment, and $\phi_{J'}^n(R)$ is a bound-state eigensolution with eigenvalue E_{nJ} . The continuum functions are energy normalized so that

$$\lim_{R \rightarrow \infty} f_J(kR) \sim \sqrt{\frac{2\mu}{\pi k}} \sin(kR + \delta_J - J\pi/2), \quad (10)$$

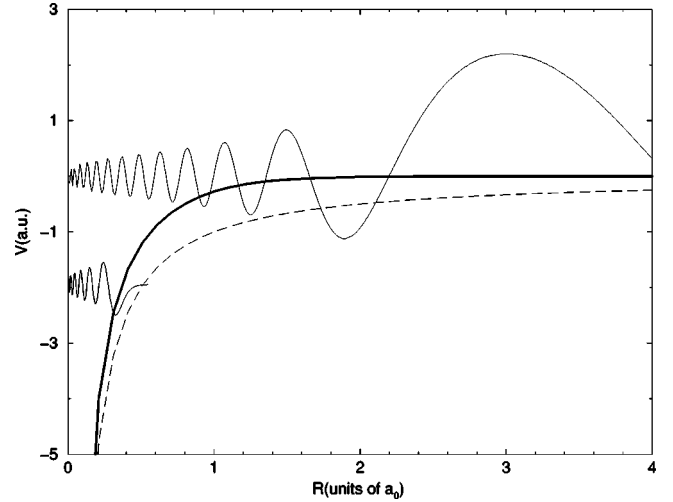


FIG. 1. Plot of the hydrogen-antihydrogen Born-Oppenheimer potential (solid line), shifted so that its asymptotic value is null, and the $p\bar{p}$ Coulomb potential (dashed line). The two dotted lines correspond to a continuum radial wave function that is a solution to Eq. (9), and the $n=12$, p -wave quasibound state of the $\text{H}\bar{\text{H}}$ complex. The wave functions are expressed in arbitrary units, and the undulations near the origin at $R < 0.1a_0$, are not resolved in the figure.

where δ_J is the elastic-scattering phase shift for the J th partial wave. If we restrict our discussion to temperatures $T < 1$ K, only s waves in the incoming channel contribute and the sum over partial waves is truncated to include only the $J'=1$ contribution. In order to evaluate the sum in Eq. (7), we need to calculate all the $J'=1$, or p -wave, bound states supported by the $\text{H}\bar{\text{H}}$ ground-state potential. The $\text{H}\bar{\text{H}}$ ground-state potential is shown in Fig. 1. The details of its calculation have been discussed in a previous report [5]. The quantum numbers for the states $\phi_{J=1}^n(R)$ are listed in Table I. In that table, we also list the wavelengths λ_n of the emitted photons during recombination, in the limit $T \rightarrow 0$, to the quasibound states of the $\text{H}\bar{\text{H}}$ complex.

We simplify the evaluation of $\sigma(k)$ by using the fact that, at cold temperatures, the radial continuum function $f_J(kR)$ is independent, except for a normalization constant, of the wave number k . In the limit $k \rightarrow 0$, we express $f_J(kR)$ in the region $R < R_0$, where R_0 is a cutoff radius determined by the condition that $2\mu V(R_0) < k^2$,

$$f_{J=0}(kR) = \sqrt{\frac{2\mu k}{\pi}} \phi(R), \quad (11)$$

and $\phi(R)$ is a solution to the Schrödinger Eq. (9) for $k=0$, subject to the boundary conditions $\phi(R=0)=0$; $d\phi(R)/dR|_{R_0}=1$. $f_{J=0}(kR)$ given by expression (11) has the asymptotic form required by the effective range expansion $f_J(kR) \rightarrow \sqrt{2\mu k/\pi} \phi(R-a)$, as $R \rightarrow \infty$, where a is the scattering length. In Fig. 1 we illustrate the calculated s -wave continuum function for $k=0$ and the $n=12$ p -wave bound-

TABLE I. Bound, $J=1$, states of the ground BO potential for the $H\bar{H}$ quasimolecule. n is the principal quantum number where $n-1$ corresponds to the number of nodes in the radial wave function, $-E_n$ is the energy eigenvalue measured with respect to the asymptotic energy $V(\infty) = -1.0$ a.u., in atomic units, of the $H + \bar{H}$ system, and λ_n is the wavelength of the emitted photon, in nanometers, corresponding to association into level n at $T \rightarrow 0$.

n	$-E_n$ (a.u.)	λ_n (nm)
1	113.991	0.39971
2	50.2349	0.90701
3	27.9203	1.63191
4	17.5919	2.59002
5	11.9814	3.80284
6	8.59842	5.29904
7	6.40275	7.11622
8	4.89743	9.30353
9	3.82069	11.9254
10	3.02405	15.0670
11	2.41821	18.8418
12	1.94680	23.4043
13	1.57292	28.9674
14	1.27153	35.8335
15	1.02523	44.4421
16	0.82163	55.4549
17	0.65182	69.9018
18	0.50934	89.4554
19	0.38966	116.9303
20	0.28961	157.3273
21	0.20697	220.1481
22	0.14005	325.3297
23	0.08748	520.8639
24	0.04806	948.0682
25	0.02081	2188.96
26	0.005049	9022.81

state solution. For $T < 1$ K, expression (11) provides a convenient and accurate representation for the incoming radial wave function.

Combining Eq. (7) with expression (11), we obtain

$$\sigma(k) = \sum_n \frac{128}{3} \frac{\pi^4 v^3 \mu}{c^3 k} \left| \int_0^{R_0} dR \phi(R) D(R) \phi'_{j',=1}(R) \right|^2. \quad (12)$$

According to Eq. (12), $\sigma(k)$ diverges in the limit as the collision velocity approaches zero, a result that is consistent with the Wigner threshold law.

III. DIPOLE MOMENT

According to Eqs. (7) and (8), the propensity for radiative association is determined by the value of the electric-dipole moment that is induced by the slow approach of the H and \bar{H} atoms in their ground state.

The electric-dipole moment for the H_2 system vanishes

due to the inversion symmetry of the electronic wave functions. Because inversion symmetry is not present in the $H + \bar{H}$ system, a nonvanishing dipole moment can be induced. Below, we present both a qualitative and quantitative discussion and a calculation for the electric dipole moment in the ground $H + \bar{H}$ system.

In an inertial coordinate frame, let $\mathbf{R}_p, \mathbf{R}_{\bar{p}}$ represent the coordinates for the proton and antiproton, respectively, and let $\mathbf{x}_e, \mathbf{x}_{\bar{e}}$ represent the electronic and positronic coordinates, respectively. We define the electric-dipole operator

$$\mathbf{D} \equiv -|e|\mathbf{x}_e - |e|\mathbf{R}_p + |e|\mathbf{x}_{\bar{e}} + |e|\mathbf{R}_{\bar{p}}. \quad (13)$$

Introducing molecular coordinates,

$$\begin{aligned} \mathbf{R} &\equiv \mathbf{R}_{\bar{p}} - \mathbf{R}_p, \\ \mathbf{r}_e &\equiv \mathbf{x}_e - \frac{\mathbf{R}_p + \mathbf{R}_{\bar{p}}}{2}, \\ \mathbf{r}_{\bar{e}} &\equiv \mathbf{x}_{\bar{e}} - \frac{\mathbf{R}_p + \mathbf{R}_{\bar{p}}}{2}, \end{aligned} \quad (14)$$

then

$$\mathbf{D} = -|e|\mathbf{r}_e + |e|\mathbf{r}_{\bar{e}} - |e|\mathbf{R}. \quad (15)$$

In the Born-Oppenheimer (BO) approximation, the dipole moment is the expectation value of \mathbf{D} with respect to the ground state of the leptonic Hamiltonian,

$$\mathbf{D}(\mathbf{R}) = \langle \Psi | -|e|\mathbf{r}_e + |e|\mathbf{r}_{\bar{e}} | \Psi \rangle - |e|\mathbf{R}, \quad (16)$$

where $|\Psi\rangle$ is the lepton eigenstate. We define a molecular frame with the z axis along the interbaryon vector and find that, by symmetry, the components of \mathbf{D} along the x and y axes vanish. However, because there is no inversion symmetry along the z axis, this component does not vanish. We get

$$D(R) = \langle \Psi(R) | -|e|z_e + |e|z_{\bar{e}} | \Psi(R) \rangle - |e|R, \quad (17)$$

where R is the interbaryon distance, $z_e, z_{\bar{e}}$ are the components of the electron and positron coordinates along the molecular z axis (interbaryon axis), and $|\Psi(R)\rangle$ is the BO wave function. The BO wave function $|\Psi(R)\rangle$ is an eigenstate of the symmetry operation that involves the interchange of lepton coordinates, followed by reflection through the plane that is perpendicular to the molecular z axis [9]. The dipole operator is even under the operation and this symmetry does not prevent a nonvanishing dipole moment. Expression (17) is invariant under a translation of the origin for the lepton coordinates along the interbaryon axis.

For large R ,

$$\begin{aligned} -\langle \Psi | |e|z_e | \Psi \rangle &\rightarrow |e| \frac{R}{2}, \\ \langle \Psi | |e|z_{\bar{e}} | \Psi \rangle &\rightarrow |e| \frac{R}{2}, \end{aligned} \quad (18)$$

and so $D(R) \rightarrow 0$ as $R \rightarrow \infty$.

The leptonic dipole moment is calculated using the Born-Oppenheimer wave functions described in [5], where symmetry constraints are discussed. The BO wave functions take the form

$$\Psi(\mathbf{r}_e \mathbf{r}_e; R) = \sum_i c_i \exp[-\alpha(\lambda_1 + \lambda_2) - \beta(\mu_1 - \mu_2)] \lambda_1^{p_i} \lambda_2^{s_i} \mu_1^{q_i} \mu_2^{t_i} r_{12}^{m_i}, \quad (19)$$

where λ_i, μ_i are the prolate spheroidal coordinates

$$\lambda_i \equiv \frac{(r_{ia} + r_{ib})}{R}, \quad (20)$$

$$\mu_i \equiv \frac{(r_{ia} - r_{ib})}{R},$$

and r_{1a}, r_{1b} are the distance from the proton and antiproton, respectively, and r_{2a}, r_{2b} are the corresponding distances for the positron. The proton is located at $-R/2$ and the antiproton at $R/2$ along the z axis. The parameters $\alpha, \beta, c_i, p_i, s_i, t_i, q_i, m_i$ are variational parameters chosen to minimize the BO eigenvalue.

For a qualitative description at larger interbaryon separations, we use the simplified approximation

$$\Psi(\mathbf{r}_e \mathbf{r}_e; R) \approx N \exp[-\alpha(\lambda_1 + \lambda_2) - \beta(\mu_1 - \mu_2)] \quad (21)$$

that contains only two variational screening parameters α, β . A tabulation for the optimal parameters has been given [13]. Using the normalized form for Eq. (21), integral (17) can be performed analytically and leads to the result

$$D(R) = 2\beta[-3\alpha^2(1+2\alpha) + (3+6\alpha + 4\alpha^2)\beta^2]R \cosh(2\beta) + (3\beta^2 + \alpha\{6\beta^2 - \alpha[3+2\alpha(3+4\beta^2)]\}) / \{R \sinh(2\beta) 4\alpha\beta[2\alpha^2\beta \cosh(2\beta) + (-\alpha^2 + \beta^2 + 2\alpha\beta^2)\sinh(2\beta)]\}. \quad (22)$$

Using the linear fit $\alpha = 0.5375R - 0.2175$, $\beta = 0.44R + 0.26$, to the tabulated data [13], Eq. (22) predicts values for $D(R)$ that are shown in Fig. 2.

In Fig. 3, we plot a cross section, along the xz plane that intersects the y coordinate at the origin, of the electronic density $\int d^3\mathbf{r}_d |\Psi(\mathbf{r}_e \mathbf{r}_e; R)|^2$ obtained using Eq. (21) at some interbaryon separation R . In that figure the proton is located at $-R/2$ for $R = 1a_0$ but the center of electronic charge is offset somewhat from the proton's location. The electron cloud is polarized by the repulsive force induced by the antiproton, and though the positron cloud has an attractive influence, it is diffuse and does not compensate for the electron-antiproton repulsion. The net effect is that a dipole is induced in the hydrogen atom. At the same time, the positron cloud (see dashed line) is also polarized and leads to a

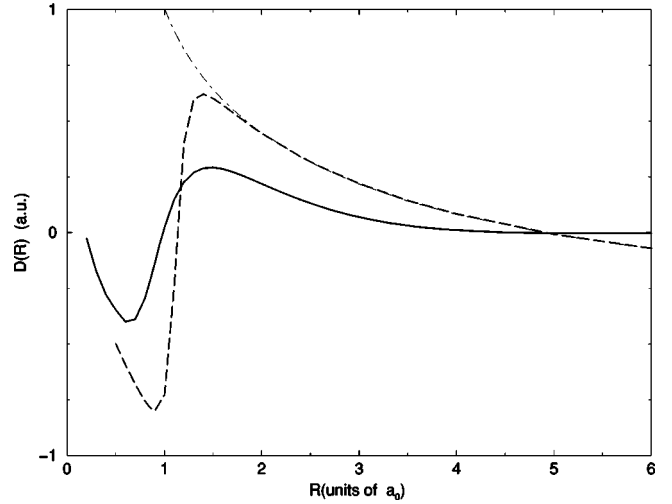


FIG. 2. Plot of the radial dipole moment $D(R)$ expressed in atomic units. The alternating long-short dashed line represents the dipole obtained using the approximation given by formula (21), and the dashed line is the dipole moment obtained using ansatz (23). The solid line represents the dipole moment obtained using the accurate representation (19) for the ground-state BO wave function. These values have been adopted for use in our calculations for the association cross sections, and for $R < 0.60a_0$ we use the analytic form $D(R) = -R + 0.6R^2 - 0.1R^3$ which joins smoothly with the tabulated values.

dipole moment of equal sign and magnitude to the one induced in the hydrogen atom. Therefore, the total dipole moment of the $H + \bar{H}$ is nonzero.

The above description is invalid at small internuclear distances since in that region ansatz (21), describing leptons

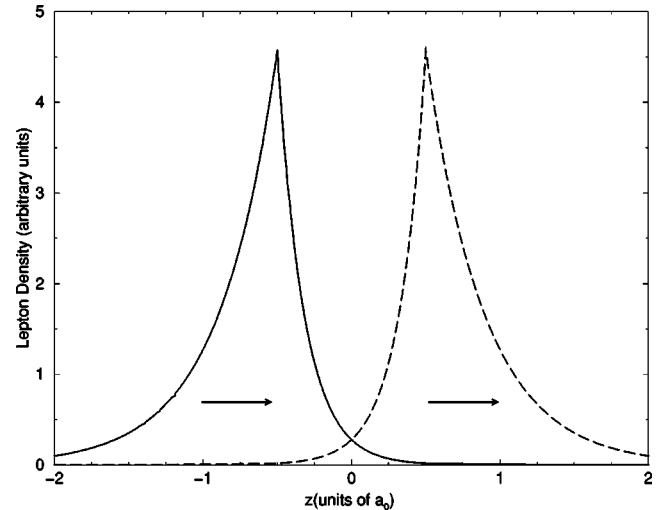


FIG. 3. Illustration of the electron charge density (solid line) and positron charge density (dashed line), obtained using the approximate form Eq. (21) for the lepton wave function. The cusps correspond to the position of the nuclei at $R = -0.5a_0$ for the proton and $R = 0.5a_0$ for the antiproton. The tail of the arrow, below the solid line, shows the center of electronic charge (magnified here for the sake of illustration), and the head shows the center of positive charge, the location of the proton. The arrow under the dashed line represents the dipole moment induced in the antihydrogen atom.

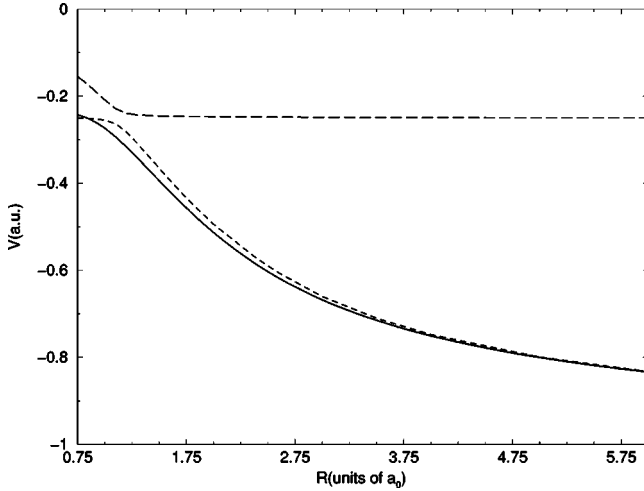


FIG. 4. Plot of the eigenvalues corresponding to the roots of the secular equation obtained from Eq. (25). The flat dashed line represents the eigenvalue corresponding to the bound positronium fragment, whereas the lower root represents the BO eigenvalue of the ground $H-\bar{H}$ fragment. The solid line is an accurate representation of the lepton BO eigenvalue for the ground state, discussed in detail elsewhere [5].

bound to their centers, is not appropriate. At a critical interbaryon separation [14], the leptons are ejected as it is energetically favorable for them to form a bound positronium. This behavior can be illustrated by an approximate BO wave function of a form that allows for fragmentation,

$$|\Psi\rangle = \frac{1}{\sqrt{2}}[\sin\theta|e^+e^-\rangle + \cos\theta|\text{BO}'\rangle], \quad (23)$$

where $|e^+e^-\rangle$ is a cavity-normalized positronium wave function describing a $1s$ positronium atom at rest, θ is a mixing parameter, and $|\text{BO}'\rangle$ is a normalized leptonic function that is orthogonal to the $|e^+e^-\rangle$ fragment, i.e.,

$$|\text{BO}'\rangle = (1 - |e^+e^-\rangle\langle e^-e^+|)|\text{BO}\rangle, \quad (24)$$

where $|\text{BO}\rangle$ is the variational function (21). We note that $\langle e^+e^-|\text{BO}'\rangle = 0$ and we renormalize $|\text{BO}'\rangle$ so that $\langle \text{BO}'|\text{BO}'\rangle = 1$. We use Eq. (23) as an improved trial wave function that leads to the following eigenvalue equation:

$$\begin{pmatrix} \langle e^-e^+|\text{H}|e^+e^-\rangle & \langle e^-e^+|\text{H}|\text{BO}'\rangle \\ \langle \text{BO}'|\text{H}|e^+e^-\rangle & \langle \text{BO}'|\text{H}|\text{BO}'\rangle \end{pmatrix} \begin{pmatrix} \sin\theta \\ \cos\theta \end{pmatrix} = E \begin{pmatrix} \sin\theta \\ \cos\theta \end{pmatrix}, \quad (25)$$

where H is the leptonic Hamiltonian. The roots of the secular equation are plotted in Fig. 4. They are illustrated by the dashed lines and correspond to the ground state and the positronium fragment lepton energy, respectively. The solid line represents the ground-state energy that was obtained using the more accurate variational function (19). Using the solution to Eq. (25) that corresponds to the lowest root of the secular equation, we construct the dipole moment by taking the expectation value (17). The result is plotted in Fig. 2 and is represented by the long dashed line. At large R , the dipole

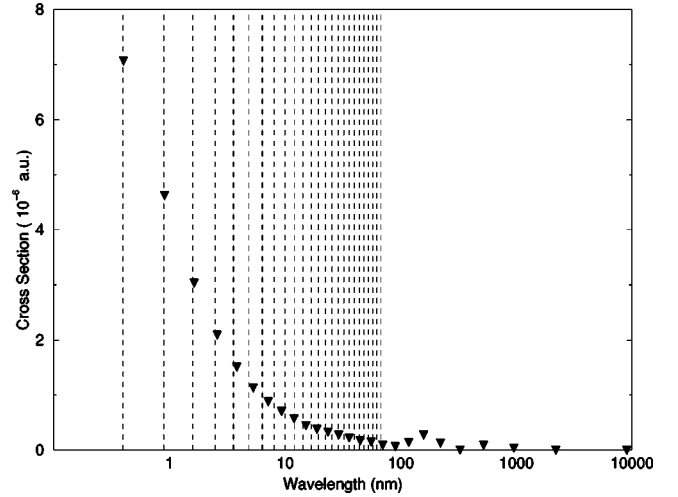


FIG. 5. Plot of the partial cross sections, represented by the filled triangles, at $T=1$ K, for the process $H+\bar{H}\rightarrow H\bar{H}(n)+h\nu_n$. The quasibound states $H\bar{H}(n)$, into which association occurs, are listed in Table I. The abscissa is the wavelength λ_n of the emitted photon in decay into state n . The cross sections for effective temperatures $T < 1$ K can be obtained by scaling the cross sections shown in Fig. 5 by the factor $1/\sqrt{T}$, where T is given in units of Kelvin. The dashed vertical lines represent the wavelengths for the radiation emitted by association of protons with antiprotons. Only the first two dozen or so lines are shown in the figure.

moments predicted using approximations (21) and (23) are in harmony, but at smaller R the positronium component in ansatz (23) has a dramatic effect. At a critical value for R , the leptonic function assumes mostly an $|e^+e^-\rangle$ character, and as R decreases, the lepton expectation value of the dipole operator in expression (17) assumes a value of equal magnitude but opposite sign to the baryon contribution $-|e|R$. At this point, $D(R)$ undergoes the sign change that is evident in Fig. 2. At still smaller R , the lepton contribution is negligible and the total dipole moment is dominated by the baryon contribution. The solid line in Fig. 2 represents the values for $D(R)$ obtained using ansatz (19) and they are the values we adopted to calculate the radiative rate coefficients. We note that expression (19) does not explicitly contain $|e^+e^-\rangle$ fragments but they are implicitly incorporated into the ansatz because of its functional dependence on r_{12} . For $R > 0.85a_0$, Fig. 4 shows that ansatz (19) is superior, as expected, to ansatz (23) but the latter provides a better description for $R \lesssim 0.75a_0$.

The integrals involved in the calculation of overlaps between the $|e^-e^+\rangle$ and $|\text{BO}\rangle$ functions involve different lepton arrangements and are not trivial. In order to calculate the integrals used in constructing the matrix elements in Eq. (25), we employed Monte Carlo integration in a six-dimensional spherical cavity. The free positronium state was described using cavity-normalized functions.

IV. RESULTS AND DISCUSSION

The results of the cross-section calculations are illustrated in Fig. 5, where we plot the partial cross sections $\sigma(n)$ corresponding to radiative recombination into the quasibound

state n of the $\text{H}\bar{\text{H}}$ complex at the effective temperature $T = 1$ K. The cross sections are expressed as a function of an effective temperature, where $E \equiv \kappa T$ is the collision energy for the relative motion of the $\text{H} + \bar{\text{H}}$ atoms, κ is the Boltzmann constant, and T is the temperature expressed in units of Kelvin. The total cross section is the sum $\sum_n \sigma(n)$, where n extends over all quantum numbers listed in Table I. At 1 K, it has the value $\sigma = 6.85 \times 10^{-22}$ cm². For temperatures below 1 K, the partial cross sections can be obtained by scaling the values shown in Fig. 5 by the factor $1/\sqrt{T}$. The figure shows that decay into the lowest p state of the $\text{H}\bar{\text{H}}$ complex, resulting in the emission of a 0.399 71-nm photon, is the dominant line emission. This occurs because the ν^3 factor in Eq. (12) is largest for this state. With increasing n , the ν^3 factor flattens to the progressively decreasing emission intensities, evident in Fig. 5, for radiative capture into higher-energy states. The eigenvalue for the $n = 1, J = 1$ bound-state solution to the $\text{H}\bar{\text{H}}$ BO potential is $E = -113.991$ a.u., whereas the eigenvalue for the first, $J = 1$, bound state of protonium is $E = -114.76$ a.u. [Both energies are taken with respect to the respective ground-state separated atom limits, i.e., $V(\infty) = -1.0$ a.u. for $\text{H}\bar{\text{H}}$ and $V(\infty) = 0.0$ a.u. for $p\bar{p}$.] The radiative association process $p + \bar{p} \rightarrow p\bar{p} + h\nu$, where $p\bar{p}$ is in the first $J = 1$ state, results in the emission of a 0.397 034 nm photon. In Fig. 5, we also plot, represented by the dashed vertical lines, the locations of emission lines for the related process $p + \bar{p} \rightarrow p\bar{p} + h\nu$. Only the first two dozen or so lines, for protonium recombination, are shown in the figure. Because protonium is a pure Coulombic system, the lines share the telltale structure of an increasingly dense set of neighboring lines due to capture into Rydberg states, seen in Coulomb systems. From Fig. 5 and Table I, we conclude that the spectrum resulting from the radiative association of H with $\bar{\text{H}}$ can be distinguished, in the wavelength region from about 1 nm to 100 nm, from the spectrum associated with the recombination of a proton with an antiproton.

The process $\text{H} + \bar{\text{H}} \rightarrow \text{H}\bar{\text{H}} + h\nu$ may provide a valuable diagnostic for hydrogen-antihydrogen interactions, as an unambiguous detection scheme to measure the presence of antihydrogen in a sample of a cold hydrogen/antihydrogen gas. Presently, the ATHENA experiment [2] at the CERN AD facility proposes to use gamma-ray detection of photons resulting from the annihilation of electrons and positrons in order to detect the presence of antihydrogen in the trapped sample. Since the detection of the back-to-back 511-keV gamma-ray radiation is an indicator only of the presence of positrons, an unambiguous signature for antihydrogen appears to be required by the simultaneous detection of heavy particle fragments [2]. Our results suggest that the measure-

ment of the spectrum shown in Fig. 5 offers an alternative, direct and unambiguous, approach for detecting the presence of trapped antihydrogen. In addition to detection of the recombination lines, the fact that the $\text{H}\bar{\text{H}}$ ground state possesses a nonvanishing electric-dipole moment could allow spectroscopic study of the electric-dipole radiation resulting from transitions among the quasibound states of this complex.

The quasibound states of the $\text{H}\bar{\text{H}}$ molecule are unstable with respect to annihilation, but since that rate depends on the value of the electron/positron wave function at the point of coalescence, or at the proton/antiproton coalescence point, highly excited, non- s -wave states of the $\text{H}\bar{\text{H}}$ could conceivably have long lifetimes with respect to annihilation. However, the bound states of $\text{H}\bar{\text{H}}$ lie in a continuum that separates to a positronium and can decay into it in a process analogous to molecular preionization. The line profile will be modified by the interaction. Estimates for the latter can be obtained by the application of a multichannel collision theory. In addition, a multichannel description will allow the accurate determination of the imaginary component of the elastic phase shift, in the wave function given by Eq. (10), that is induced by the loss processes itemized in the Introduction. An imaginary component in the elastic phase shift affects the value of the overlap integrals in Eq. (12) and hence alters the value of the radiative cross section from that shown in Fig. 5. Preliminary estimates suggest that this effect is small, but an accurate assessment requires the implementation of the multichannel scattering theory.

The association process (6) offers a possible route for the creation of a novel molecule, the quasibound $\text{H}\bar{\text{H}}$ system. The rate can be enhanced, over the values reported here, by the application of a laser field to stimulate the association process [12,15,16]. Work in progress includes calculation for association into higher angular momentum states of the $\text{H}\bar{\text{H}}$ complex. They could be more stable with respect to the annihilation, but direct association into these levels can only be achieved at temperatures greater than 1 K.

ACKNOWLEDGMENTS

B.Z. was supported by the National Science Foundation through grants from the Smithsonian Institution and Harvard University for the Institute for Theoretical Atomic and Molecular Physics (ITAMP). B.Z. also thanks the Sabbatical Committee at the University of Nevada, Las Vegas for allowing a sabbatical leave to ITAMP. A.D. was supported by the U.S. Department of Energy, Office of Basic Energy Sciences.

-
- [1] G. Bauer *et al.*, Phys. Lett. B **368**, 251 (1996).
 [2] M. H. Holzscheiter and M. Charlton, Rep. Prog. Phys. **62**, 1 (1999).
 [3] D. Kleppner (private communication).
 [4] P. Froelich, S. Jonsell, A. Saenz, B. Zygelman, and A. Dal-

- garno, Phys. Rev. Lett. **84**, 4577 (2000).
 [5] S. Jonsell, A. Saenz, P. Froelich, B. Zygelman, and A. Dalgarno (unpublished).
 [6] D. L. Morgan and V. W. Hughes, Phys. Rev. D **2**, 1389 (1970).

- [7] B. R. Junker and J. N. Bardsley, Phys. Rev. Lett. **28**, 1227 (1972).
- [8] D. L. Morgan and V. W. Hughes, Phys. Rev. A **7**, 1811 (1973).
- [9] W. Kolos, D. Morgan, D. Schrader, and L. Wolniewicz, Phys. Rev. A **11**, 1792 (1975).
- [10] A. Yu. Voronin and J. Carbonell, Phys. Rev. A **57**, 4335 (1998).
- [11] P. K. Sinha and A. S. Gosh, Europhys. Lett. **49**, 558 (2000).
- [12] B. Zygelman, P. C. Stancil, and A. Dalgarno, Ap. J. **508**, 151 (1998).
- [13] R. I. Campeanu and T. Beu, Phys. Lett. **93A**, 223 (1983).
- [14] E. A. G. Armour, J. M. Carr, and V. Zeman, J. Phys. B **31**, L679 (1998).
- [15] F. B. Yousif, P. Van der Donk, Z. Kuchеровsky, J. Reis, E. Brannen, J. B. A. Mitchell, and T. J. Morgan, Phys. Rev. Lett. **67**, 26 (1991).
- [16] R. Wynar, R. S. Freeland, D. J. Han, C. Ryu, and D. J. Heinzen, Science **287**, 1016 (2000).